ARCHIVES OF ELECTRICAL ENGINEERING VOL. 70(2), pp. 445–462 (2021)

DOI 10.24425/aee.2021.136995

Dynamic interactions stability analysis of hybrid renewable energy system with SSSC

Ping He, Pan Qi, Yuqi Ji, Zhao Li

Zhengzhou University of Light Industry
No.5 Dongfeng Road, Jinshui District, Zhengzhou, 450002, China
e-mail: hplkz@126.com

(Received: 26.09.2020, revised: 21.12.2020)

Abstract: The static series synchronous compensator (SSSC) has demonstrated its capability in providing voltage support and improving power system stability. The objective of this paper is to analyze the dynamic interaction stability mechanism of a hybrid renewable energy system connected with doubly-fed induction generators (DFIGs) and solid oxide fuel cell (SOFC) energy with the SSSC. For this purpose, a linearized mathematical model of this modified hybrid single-machine infinite-bus (SMIB) power system is developed to analyze the physical mechanism of the SSSC in suppressing oscillations and the influence on the dynamic stability characteristics of synchronization. Typical impacting factors such as the series compensation level, the SOFC penetration and tie-line power are considered in the SMIB and two-area systems. The impact of dynamic interactions on enhancing damping characteristics and improving transient performance of the studied systems is demonstrated using eigenvalue analysis and dynamic time-domain simulations, which validates the validity of the proposed physical mechanism simultaneously.

Key words: damping characteristics, dynamic interaction analysis, eigenvalue analysis, hybrid renewable energy system, SSSC

1. Introduction

Recently, renewable energy sources have been utilized to ease the depletion of fossil energy deposits, while numerous measures have been taken to conquer the severe environmental issues caused by combustions of fossil fuels [1]. For instance, wind power generators, which are mainly doubly-fed induction generators (DFIG), widely integrated into modern power systems and expected to supply 20% of global electricity by 2030 [2], and the solid oxide fuel cell (SOFC), due to its modular, efficient and non-polluting characteristics, are two promising options of clean energy sources. Considering the rapid development and great potentiality of SOFC technology,

it will have a capital effect on a modern power system in the future. Therefore, the analysis of stability for the hybrid power system connected with DFIG and SOFC energy is essential and vital. In spite of the benefits of wind power and SOFC generation, new challenges with respect to stability appear [3–6], and the low-frequency oscillation phenomena of such a hybrid power system is inevitable, especially an interconnected one. Thus, the dynamic interaction stability of the power generation by DFIG and SOFC energy should be carefully examined.

The well-known flexible alternating current transmission system (FACTS) device is very efficient in contributing to voltage stability and oscillation damping improvement. Due to its flexibility and capability in controlling power system dynamics, the FACTS device has been employed for voltage support and stability improvement [7, 8], as well as for controlling power flow [9] and minimizing power losses in transmission systems [10]. An oscillation damping controller (ODC) of a static series synchronous compensator (SSSC) is designed by using modal control theory to improve the stability and achieve power control of a single-machine infinite-bus (SMIB) system integrated a DFIG-based wind farm using an SSSC in Reference [11]. It is concluded in [12] that the static synchronous compensator (STATCOM) can improve the transient voltage stability and helps the wind turbine generators and fuel cell system to remain in service during grid faults. A hybrid Firefly Algorithm and Pattern Search strategy is employed for an SSSC-based power oscillation controller design in Reference [13]. In Reference [14], the research results on improving power oscillation damping and increased transmission capacities under dynamic conditions using SSSC technology is discussed. A multi-objective predictive control strategy is carried out for the stability improvement of a power system connected with wind farms using the STATCOM in [15]. The research work in Reference [16] presents the transient stability and low voltage ride through the improvement of the IEEE 68-bus system connected with wind farms and photovoltaic plants through coordination of SSSC and power system stabilizer (PSS) controllers. To supply adequate damping characteristics to a hybrid DFIG-based and permanent magnet generator-based wind farms, an adaptive-network-based fuzzy inference system controller of an SSSC is proposed in [17]. The SSSC based damping controllers in [18] is proposed to improve the reactive power and the damping performance of the system in the event of a major disturbance. The fractional-order multi-input single-output SSSC using a whale optimization algorithm is produced to improve power system stability in [19].

The existing researches mainly focus on the control strategies to improve the system stability. There are few literatures to analyze the physical mechanism in suppressing oscillations and the influence on the dynamic characteristics of synchronization in a hybrid power system connected with DFIG and SOFC energy. Given this background, the following issues are addressed in this work:

- The proposed system contains a hybrid structure, including a synchronous generator, the DFIG-based wind farm, SOFC and SSSC.
- The linearized mathematical model of this modified hybrid SMIB power system is developed, and the details of the physical mechanism are presented from the perspective of total damping.
- Typical impacting factors such as the series compensation level, the SOFC penetration and tie-line power are considered as part of the stability analysis of this hybrid SMIB system or the two-area system. In addition, we adopt the constant voltage control strategy regarding the control of the SSSC for improving the system stability.

The structure of this paper is as follows. The configuration of the hybrid SMIB system and models being considered are presented in Section 2. The detailed process of building the linearized mathematical model of this modified SMIB system and the analysis of the dynamic interactions for the SMIB system are depicted in Section 3. To demonstrate the impact of the dynamic of the hybrid power system connected with DFIG and SOFC energy as well as with the SSSC, the eigenvalue analysis and dynamic time-domain simulations are examined in Section 4. Finally, some conclusions are drawn in Section 5.

2. Configuration of the hybrid SMIB system and model being considered

The configuration of the studied system is presented in Fig. 1. The synchronous generator (SG), aggregated wind farm, and aggregated SOFC power plant are connected to an infinite bus through a step-up transformer and a transmission line, respectively. The transmission line contains an SSSC. The equivalent wind DFIG is driven by an equivalent wind turbine through an equivalent gearbox (GB). The aggregated SOFC power plant is shown by SOFC stack connected to Bus 3 via a dc-dc converter and a voltage-source inverter (VSI) coupled by a dc capacitor. The employed mathematical models of the power system are described hereafter.

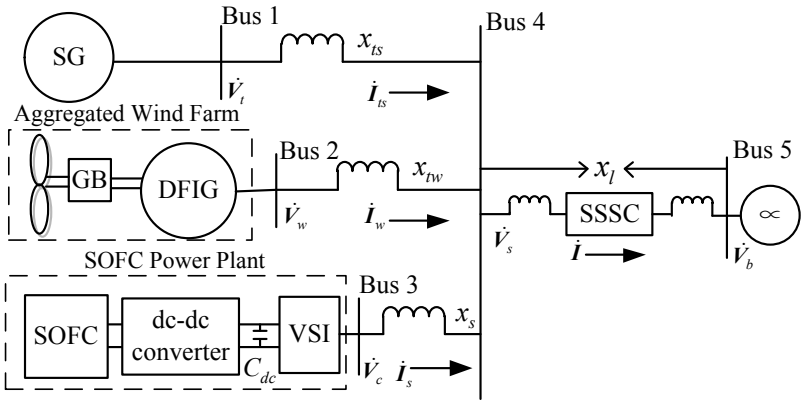

Fig. 1. Single-line diagram of the studied system

2.1. SG model

The SG model used in this paper can be illustrated by [20]:

$$\begin{cases} p(\delta) = \omega - \omega_0 \\ p(\omega) = \dfrac{1}{T_J}\left(P_m - P_e\right) \\ p\left(E'_q\right) = \dfrac{1}{T'_{d0}}\left(E_{ge} - E_q\right) \\ p\left(E_{qe}\right) = \dfrac{-E_{qe}}{T_a} + \dfrac{K_a}{T_a}\left(V_{t\text{ref}} - V_t\right) \end{cases}, \tag{1}$$

where:

$$\begin{cases} P_e = E'_q I_{tsq} + \left(x_q - x'_d\right) I_{tsd} I_{tsq} \\ E_q = E'_q + \left(x_d - x'_d\right) I_{tsd} \\ V_t = \sqrt{V_{td}^2 + V_{tq}^2} = \sqrt{\left(x_q I_{tsq}\right)^2 + \left(E'_q - x'_d I_{tsd}\right)^2} \end{cases} \tag{2}$$

and where δ is the rotor angle; ω is the SG rotor angular speed; ω_0 is the synchronous angular speed; T_J is the inertia time constant; T is the time constant of the excitation circuit; T_a is the regulator time constant; P_m and P_e are the input mechanical power and output electrical power, respectively; E'_q is the q-axis behind transient voltage; E_{qe} is the generator field voltage; E_q is the no-load electromotive force; K_a is the regulator gain; V_t and $V_{t\,\mathrm{ref}}$ are the terminal voltage and required voltage, respectively; x_d and x_q are the d- and q-axis synchronous reactances, respectively; x'_d is the d-axis transient reactance; I_{tsd} and I_{tsq} are the d- and q-axis stator currents of the SG, respectively; V_{td} and V_{tq} are the d- and q-axis terminal voltages of the SG, respectively; p is the differential operator with respect to time t.

2.2. DFIG wind farm model

For the normal dynamic model configuration of a DFIG wind farm, the wind speed model, wind power model, mechanical drive train, DFIG model, pitch controller, rotational speed controller, and converter controllers are included, as depicted in Fig. 2.

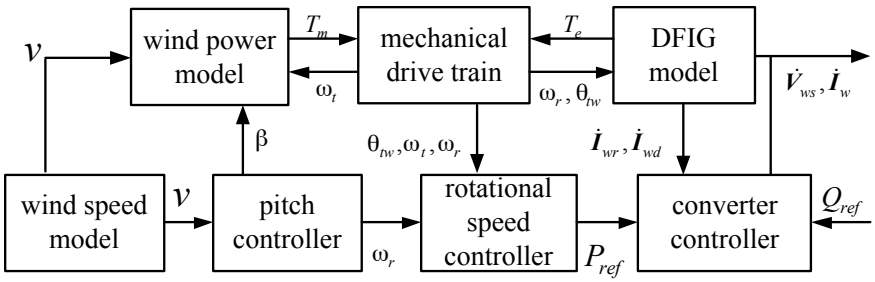

Fig. 2. Dynamic model configuration of DFIG-based wind farm

The detailed mathematical models and the associated control schemes of the controllers can be found in [21,22] and only the following differential algebraic equations are given here to study the dynamic interaction stability analysis of the studied hybrid system.

$$
\begin{cases}
p\left(i_{wds}\right) = -\dfrac{\omega_s}{X_s'}\left(R_s + \dfrac{X_s - X_s'}{\omega_s T_0'}\right) i_{wds} + \omega_s i_{wqs} - \\
\qquad -\dfrac{\omega_r e_d'}{X_s'} + \dfrac{e_q'}{X_s' T_0'} + \dfrac{\omega_s V_{wds}}{X_s'} - \dfrac{\omega_s L_m V_{wdr}}{X_s' L_{rr}} \\
p\left(i_{wqs}\right) = -\omega_s i_{wds} - \dfrac{\omega_s}{X_s'}\left(R_s + \dfrac{\left(X_s - X_s'\right)}{\omega_s T_0'}\right) i_{wqs} - \\
\qquad -\dfrac{e_d'}{X_s' T_0'} - \dfrac{\omega_r e_q'}{X_s'} + \dfrac{\omega_s V_{wqs}}{X_s'} - \dfrac{\omega_s L_m V_{wqr}}{X_s' L_{rr}} \\
p\left(e_d'\right) = -\dfrac{\left(X_s - X_s'\right) i_{wqs}}{T_0'} - \dfrac{e_d'}{T_0'} + \left(\omega_s - \omega_r\right) e_q' - \dfrac{\omega_s L_m V_{wqr}}{L_{rr}} \\
p\left(e_q'\right) = -\dfrac{\left(X_s - X_s'\right) i_{wds}}{T_0'} - \dfrac{e_q'}{T_0'} - \left(\omega_s - \omega_r\right) e_d' + \dfrac{\omega_s L_m V_{wdr}}{L_{rr}} \\
p\left(\omega_r\right) = \dfrac{\left(T_{sh} - T_e\right)}{2H_g} \\
p\left(\omega_t\right) = \dfrac{\left(T_m - T_{sh}\right)}{2H_t} \\
p\left(\theta_{tw}\right) = \omega_t - \omega_r
\end{cases}
\tag{3}
$$

in which:

$$
T_{sh} = K_{sh}\theta_{tw} + D_{sh}\left(\omega_t - \omega_r\right), \qquad T_e = \frac{e_q' i_{wqs}}{\omega_s} + \frac{e_d' i_{wds}}{\omega_s}.
$$

where R_s is stator resistance; X_s and X_s' are the stator reactance and transient reactance of the DFIG, respectively; ω_s, ω_r, and ω_t are the DFIG stator angular speed, rotor angular speed, and the turbine angular speed, respectively; L_m and L_{rr} are the mutual inductance and rotor self-inductance, respectively; (V_{wds}, V_{wqs}) and (V_{wdr}, V_{wqr}) are the DFIG stator and rotor terminal voltages of the d- and q-axis, respectively; i_{wds} and i_{wqs} are the DFIG d- and q-axis stator currents, respectively; e_d' and e_q' are the DFIG d- and q-axis voltage behind the transient reactance, respectively; T_0', T_m, T_{sh}, and T_e are the rotor circuit time constant, the turbine input, shaft and generator torque, respectively; θ_{tw} is the shaft twist angle; K_{sh} and D_{sh} are the shaft stiffness and damping coefficients, respectively; H_t and H_g are the turbine and generator inertias, respectively.

2.3. Model of a grid-connected SOFC power plant

Power generation by fuel cells is the conversion of the chemical energy in hydrogen and oxygen directly into electricity. Fig. 3 shows the SOFC dynamic model. It contains the chemical dynamic of a fuel processor, the chemical reaction dynamic of a fuel cell stack, the fuel cell electrical dynamic, the Nernst equation, and the power electronic interface. The q_{h2-in} and q_{o2-in} are the hydrogen and oxygen input flow rates, respectively. The p_{h2}, p_{o2}, and p_{h2o} are the partial pressure for hydrogen, oxygen, and water, respectively. V_{fc} and I_{fc} are the fuel cell stack output voltage and current, respectively.

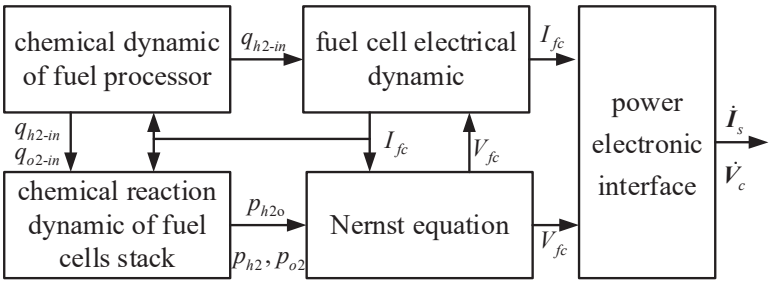

Fig. 3. Dynamic model of a grid-connected SOFC power plant

The detailed mathematical models and the associated control schemes can be found in [6,23]. The configuration of the power electronic is described in Fig. 1. The dynamic equation of the dc capacitor (C_{dc}) is written as:

$$p\left(V_{dc}\right) = \frac{1}{C_{dc}}\left[\frac{P_{fc}}{V_{dc}} - \left(I_{sd}mk\cos\psi + I_{sq}mk\sin\psi\right)\right], \tag{4}$$

where: V_{dc} is the voltage of the dc capacitor; P_{fc} is the fuel cell power; m and k are the modulation ratio and converter ratio of the VSI, respectively; I_{sd} and I_{sq} are the d- and q-axis current injected to Bus 3 (shown in Fig. 1); ψ is the phase angle of the voltage injected to Bus 3.

2.4. SSSC model

The fundamental structure of an SSSC is denoted in Fig. 4. The SSSC linked in series with the transmission line consists of a dc capacitor, a VSI and a series coupling transformer:

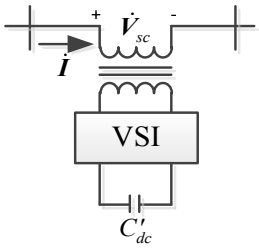

Fig. 4. Fundamental structure of an SSSC

To increase or decrease both reactive and active power flow through the transmission line, the SSSC can be operated either in capacitive or inductive mode depending on the polarity of the series injected voltage ($\dot{V}_{sc}$). Here, the SSSC works in capacitive mode to discuss its enhancement of small-signal ability, and the control for the SSSC in the process of simulation is the basic constant voltage control strategy in reference [24]. Using the synchronous reference frame, the injected voltage used in this paper can be presented as [25]:

$$\dot{V}_{sc} = V_{scd} + \mathrm{j}V_{scq} = \frac{k'm'V'_{dc}}{\sqrt{2}}\sin\delta' + \mathrm{j}\frac{k'm'V'_{dc}}{\sqrt{2}}\cos\delta' = \frac{k'm'V'_{dc}\angle\delta'}{\sqrt{2}}, \tag{5}$$

where: V_{scd} and V_{scq} are the d- and q-axis components of the injected voltage; V'_{dc} is the voltage of the dc capacitor of the SSSC; δ' is the phase angle of the injected voltage; k' is the turns ratio of the coupling transformer; m' is the modulation ratio of the inverter.

3. Linearized mathematical model and dynamic interactions analysis

3.1. Linearized mathematical model of the hybrid SMIB

The small-signal analysis is one of the effective methods of knowing the inherent dynamic characteristics of the power system through linearization techniques and eigenvalue analysis [26]. In this paper, the derived mathematical model in Section 2 is used to establish the linearization model of the studied hybrid renewable energy system with an SSSC to analyze the dynamic interactions of the linearization model of the studied hybrid renewable energy system with an SSSC.

From the configuration of the studied system, as indicated in Fig. 1, the system voltage equations are given by:

$$\begin{cases} \dot{\boldsymbol{V}}_t = \mathrm{j}x_{ts}\dot{\boldsymbol{I}}_{ts} + \dot{\boldsymbol{V}}_s \\ \dot{\boldsymbol{V}}_s = \dot{\boldsymbol{V}}_c - \mathrm{j}x_s\dot{\boldsymbol{I}}_s \\ \dot{\boldsymbol{V}}_w = \mathrm{j}x_{tw}\dot{\boldsymbol{I}}_w + \dot{\boldsymbol{V}}_s \\ \dot{\boldsymbol{V}}_s - \dot{\boldsymbol{V}}_b + \dot{\boldsymbol{V}}_{sc} = \mathrm{j}x_s\left(\dot{\boldsymbol{I}}_{ts} + \dot{\boldsymbol{I}}_s + \dot{\boldsymbol{I}}_w\right) \end{cases}, \tag{6}$$

where: $\dot{\boldsymbol{V}}_t$, $\dot{\boldsymbol{V}}_w$, $\dot{\boldsymbol{V}}_c$, $\dot{\boldsymbol{V}}_s$, and $\dot{\boldsymbol{V}}_b$ are the voltage of Bus 1, Bus 2, Bus 3, Bus 4, and Bus 5, respectively; x_{ts}, x_{tw}, x_s, and x_l represent the equivalent reactance related to various components of the studied system. From (6), we can have the following:

$$\begin{cases} \begin{bmatrix} x_l & x_s + x_l & x_l \\ x_l & x_l & x_l + x_{tw} \\ x_q + x_{ts} + x_l & x_l & x_l \end{bmatrix} \begin{bmatrix} I_{tsq} \\ I_{sq} \\ I_{wq} \end{bmatrix} = \begin{bmatrix} V_b \sin\delta - V_{sc}\sin\delta' - V_c\cos\psi \\ V_b \sin\delta - V_{sc}\sin\delta' - V_{dw} \\ V_b \sin\delta - V_{sc}\sin\delta' \end{bmatrix} \\ \begin{bmatrix} x_l & x_s + x_l & x_l \\ x_l & x_l & x_l + x_{tw} \\ x'_d + x_{ts} + x_l & x_l & x_l \end{bmatrix} \begin{bmatrix} I_{tsd} \\ I_{sd} \\ I_{wd} \end{bmatrix} = \begin{bmatrix} V_c \sin\psi - V_b\cos\delta + V_{sc}\cos\delta' \\ V_{qw} - V_b\cos\delta + V_{sc}\cos\delta' \\ E'_q - V_b\cos\delta + V_{sc}\cos\delta' \end{bmatrix} \end{cases}, \tag{7}$$

where: V_{dw} and V_{qw} are the DFIG d- and q-axis stator voltages, respectively; V_c is the amplitude of $\dot{\boldsymbol{V}}_c$, the voltage of Bus 3.

By linearization of (7), we can have:

$$\begin{cases} \begin{bmatrix} \Delta I_{tsq} \\ \Delta I_{sq} \\ \Delta I_{wq} \end{bmatrix} = \boldsymbol{A}^{-1} \times \\ \times \begin{bmatrix} V_b \cos\delta\Delta\delta - \dfrac{k' \sin\delta' V'_{dc} \Delta m'}{\sqrt{2}} - \dfrac{k' m' V'_{dc} \cos\delta' \Delta\delta'}{\sqrt{2}} - k\cos\psi\,(m\Delta V_{dc} + V_{dc}\Delta m) + kmV_{dc}\sin\psi\Delta\psi \\ V_b \cos\delta\Delta\delta - \dfrac{k' \sin\delta' V'_{dc} \Delta m'}{\sqrt{2}} - \dfrac{k' m' V'_{dc} \cos\delta' \Delta\delta'}{\sqrt{2}} - \left(\Delta e'_d - R_s \Delta i_{wds} + X'_s \Delta i_{wqs}\right) \\ V_b \cos\delta\Delta\delta - \dfrac{k' \sin\delta' V'_{dc} \Delta m'}{\sqrt{2}} - \dfrac{k' m' V'_{dc} \cos\delta' \Delta\delta'}{\sqrt{2}} \end{bmatrix} \\ \begin{bmatrix} \Delta I_{tsd} \\ \Delta I_{sd} \\ \Delta I_{wd} \end{bmatrix} = \boldsymbol{B}^{-1} \times \\ \times \begin{bmatrix} k\sin\psi\,(m\Delta V_{dc} + V_{dc}\Delta m) + kmV_{dc}\cos\psi\Delta\psi + V_b \sin\delta\Delta\delta + \dfrac{k' \cos\delta' V'_{dc} \Delta m'}{\sqrt{2}} - \dfrac{k' m' V'_{dc} \sin\delta' \Delta\delta'}{\sqrt{2}} \\ \left(\Delta e'_q - R_s \Delta i_{wqs} - X'_s \Delta i_{wds}\right) + V_b \sin\delta\Delta\delta + \dfrac{k' \cos\delta' V'_{dc} \Delta m'}{\sqrt{2}} - \dfrac{k' m' V'_{dc} \sin\delta' \Delta\delta'}{\sqrt{2}} \\ \Delta E'_q + V_b \sin\delta\Delta\delta + \dfrac{k' \cos\delta' V'_{dc} \Delta m'}{\sqrt{2}} - \dfrac{k' m' V'_{dc} \sin\delta' \Delta\delta'}{\sqrt{2}} \end{bmatrix} \end{cases} . \quad (8)$$

Equation (8) can be rewritten by:

$$\left[\begin{array}{cccccc} \Delta I_{tsq} & \Delta I_{sq} & \Delta I_{wq} & \Delta I_{tsd} & \Delta I_{sd} & \Delta I_{wd} \end{array} \right]^T = \left[\begin{array}{cc} \boldsymbol{A}^{-1}\,(\boldsymbol{C}\,\boldsymbol{X}) & \boldsymbol{B}^{-1}\,(\boldsymbol{D}\,\boldsymbol{X}) \end{array} \right]^T = \boldsymbol{F}\,\boldsymbol{X}, \quad (9)$$

where: $\boldsymbol{X} = \left[\begin{array}{cccccccccc} \Delta\delta & \Delta E'_q & \Delta V_{dc} & \Delta m & \Delta\psi & \Delta i_{wds} & \Delta i_{wqs} & \Delta e'_d & \Delta e'_q & \Delta m' \quad \Delta\delta' \end{array} \right]^T$; $\boldsymbol{A}$ and $\boldsymbol{B}$ are d- and q-axis impedance matrixes, respectively; $\boldsymbol{C}$ and $\boldsymbol{D}$ are matrices without real meaning; $\boldsymbol{F}$ is the coefficient matrix of the state variables in the linearized state equation of $d-q$ components of power system terminal current.

By considering (8), the linearization of (2) can be represented as:

$$\begin{cases} \Delta P_e = K_{p\delta}\Delta\delta + K_{pq}\Delta E'_q + K_{pdc}\Delta V_{dc} + K_{pm}\Delta m + K_{p\psi}\Delta\psi + K_{pds}\Delta i_{wds} + \\ \qquad + K_{pqs}\Delta i_{wqs} + K_{ped}\Delta e'_d + K_{peq}\Delta e'_q + K_{pm'}\Delta m' + K_{p\delta'}\Delta\delta' \\ \Delta E_q = K_{e\delta}\Delta\delta + K_{eq}\Delta E'_q + K_{edc}\Delta V_{dc} + K_{em}\Delta m + K_{e\psi}\Delta\psi + K_{eds}\Delta i_{wds} + \\ \qquad + K_{eqs}\Delta i_{wqs} + K_{eed}\Delta e'_d + K_{eeq}\Delta e'_q + K_{em'}\Delta m' + K_{e\delta'}\Delta\delta' \\ \Delta V_t = K_{v\delta}\Delta\delta + K_{vq}\Delta E'_q + K_{vdc}\Delta V_{dc} + K_{vm}\Delta m + K_{v\psi}\Delta\psi + K_{vds}\Delta i_{wds} + \\ \qquad + K_{vqs}\Delta i_{wqs} + K_{ved}\Delta e'_d + K_{veq}\Delta e'_q + K_{vm'}\Delta m' + K_{v\delta'}\Delta\delta' \end{cases} . \quad (10)$$

Then, by substituting (10) into the linearization of (1), the following equations are obtained:

$$\begin{cases} p\left(\Delta\delta\right) = \omega\Delta\omega_0 \\ p\left(\Delta\omega\right) = -\dfrac{1}{T_J}\times\left(K_{p\delta}\Delta\delta + K_{pq}\Delta E'_q + K_{pdc}\Delta V_{dc} + K_{pm}\Delta m + K_{p\psi}\Delta\psi + K_{pds}\Delta i_{wds} + \right. \\ \qquad \left. + K_{pqs}\Delta i_{wqs} + K_{ped}\Delta e'_d + K_{ped}\Delta e'_q + K_{pm'}\Delta m' + K_{p\delta'}\Delta\delta'\right) \\ p\left(\Delta E'_q\right) = \dfrac{\Delta E_{qe}}{T'_{d0}} - \dfrac{1}{T'_{d0}}\times\left(K_{e\delta}\Delta\delta + K_{eq}\Delta E'_q + K_{edc}\Delta V_{dc} + K_{em}\Delta m + K_{e\psi}\Delta\psi + \right. \\ \qquad \left. + K_{eds}\Delta i_{wds} + K_{eqs}\Delta i_{wqs} + K_{eed}\Delta e'_d + K_{eeq}\Delta e'_q + K_{em'}\Delta m' + K_{e\delta'}\Delta\delta'\right) \\ p\left(\Delta E_{qe}\right) = -\dfrac{\Delta E_{qe}}{T_a} - \dfrac{K_a}{T_a}\times\left(K_{v\delta}\Delta\delta + K_{vq}\Delta E'_q + K_{vdc}\Delta V_{dc} + K_{vm}\Delta m + K_{v\psi}\Delta\psi + \right. \\ \qquad \left. + K_{vds}\Delta i_{wds} + K_{vqs}\Delta i_{wqs} + K_{ved}\Delta e'_d + K_{ved}\Delta e'_q + K_{vm'}\Delta m' + K_{v\delta'}\Delta\delta'\right) \end{cases} . \quad (11)$$

By linearization of (3), we can have:

$$\begin{cases} p\left(\Delta i_{wds}\right) = -\dfrac{\omega_s\left(2R_s + \dfrac{\left(X_s - X'_s\right)}{\omega_s T'_0}\right)\Delta i_{wds}}{X'_s} + 2\omega_s\Delta i_{wqs} + \\ \qquad + \dfrac{\left(\omega_s - \omega_r\right)\Delta e'_d}{X'_s} + \dfrac{\Delta e'_q}{X'_s T'_0} - \dfrac{e'_d\Delta\omega_r}{X'_s} - \dfrac{\omega_s L_m\Delta V_{wdr}}{X'_s L_{rr}} \\ p\left(\Delta i_{wqs}\right) = -2\omega_s\Delta i_{wds} - \dfrac{\omega_s\left(2R_s + \dfrac{\left(X_s - X'_s\right)}{\omega_s T'_0}\right)\Delta i_{wqs}}{X'_s} - \\ \qquad - \dfrac{\Delta e'_d}{X'_s T'_0} + \dfrac{\left(\omega_s - \omega_r\right)\Delta e'_q}{X'_s} - \dfrac{e'_q\Delta\omega_r}{X'_s} - \dfrac{\omega_s L_m\Delta V_{wqr}}{X'_s L_{rr}} \\ p\left(\Delta e'_d\right) = -\left(X_s - X'_s\right)\dfrac{\Delta i_{wqs}}{T'_0} - \dfrac{\Delta e'_d}{T'_0} + \left(\omega_s - \omega_r\right)\Delta e'_q - e'_q\Delta\omega_r - \dfrac{\omega_s L_m V_{wqr}}{L_{rr}} \\ p\left(\Delta e'_q\right) = -\dfrac{\left(X_s - X'_s\right)\Delta i_{wds}}{T'_0} - \dfrac{\Delta e'_q}{T'_0} - \left(\omega_s - \omega_r\right)\Delta e'_d + e'_d\Delta\omega_r + \dfrac{\omega_s L_m V_{wdr}}{L_{rr}} \\ p\left(\Delta\omega_r\right) = -\dfrac{e'_d\Delta i_{wds}}{2H_g\omega_s} - \dfrac{e'_q\Delta i_{wqs}}{2H_g\omega_s} - \dfrac{i_{wds}\Delta e'_d}{2H_g\omega_s} + \\ \qquad - \dfrac{i_{wqs}\Delta e'_q}{2H_g\omega_s} - \dfrac{D_{sh}\Delta\omega_r}{2H_g} + \dfrac{D_{sh}\Delta\omega_t}{2H_g} + \dfrac{K_{sh}\Delta\theta_{tw}}{2H_g} \\ p\left(\Delta\omega_t\right) = \dfrac{D_{sh}\Delta\omega_r}{2H_t} - \dfrac{D_{sh}\Delta\omega_t}{2H_t} - \dfrac{K_{sh}\Delta\theta_{tw}}{2H_t} + \dfrac{\Delta T_m}{2H_t} \\ p\left(\Delta\theta_{tw}\right) = -\Delta\omega_r + \Delta\omega_t \end{cases} . \quad (12)$$

The linearization of (4) results in the following equation:

$$\begin{aligned} p\left(\Delta V_{dc}\right) = \frac{-1}{C_{dc}} \Big[& \left(a_4 f_{51} + a_5 f_{21}\right) \Delta\delta + \left(a_4 f_{52} + a_5 f_{22}\right) \Delta E'_q + \left(a_1 + a_4 f_{53} + a_5 f_{23}\right) \Delta V_{dc} + \\ & + \left(a_2 + a_4 f_{54} + a_5 f_{24}\right) \Delta m + \left(a_3 + a_4 f_{55} + a_5 f_{25}\right) \Delta\psi + \left(a_4 f_{56} + a_5 f_{26}\right) \Delta i_{wds} + \\ & + \left(a_4 f_{57} + a_5 f_{27}\right) \Delta i_{wqs} + \left(a_4 f_{58} + a_5 f_{28}\right) \Delta e'_d + \left(a_4 f_{59} + a_5 f_{29}\right) \Delta e'_q + \\ & + \left(a_4 f_{5,10} + a_5 f_{2,10}\right) \Delta m' + \left(a_4 f_{5,11} + a_5 f_{2,11}\right) \Delta\delta' \Big], \end{aligned} \tag{13}$$

where f is the element of $\boldsymbol{F}$; $a_1 = P_{fc}/V_{dc}^2$; $a_2 = kI_{sd}\cos\psi + kI_{sq}\sin\psi$; $a_3 = kmI_{sq}\cos\psi - kmI_{sd}\sin\psi$; $a_4 = km\cos\psi$; $a_5 = km\sin\psi$.

Thus, the linearization model of this studied hybrid renewable energy system is:

$$\boldsymbol{X}' = \boldsymbol{A}'\boldsymbol{X}' + \boldsymbol{B}'\boldsymbol{U}, \tag{14}$$

where:

$$\boldsymbol{X}' = \left[\Delta\delta\ \Delta\omega\ \Delta E'_q\ \Delta E_{qe}\ \Delta i_{wds}\ \Delta i_{wqs}\ \Delta e'_d\ \Delta e'_q\ \Delta\omega_r\ \Delta\omega_t\ \Delta\theta_{tw}\ \Delta V_{dc}\right]^T,$$

$$\boldsymbol{U} = \left[\Delta m\ \Delta\psi\ \Delta m'\ \Delta\delta'\ \Delta T_m\ \Delta V_{wdr}\ \Delta V_{wqr}\right]^T,$$

$\boldsymbol{A}'$ is the coefficient matrix of power system state variables; $\boldsymbol{B}'$ is the coefficient matrix of system control variables.

From (14), it can be concluded that the linearization model of the SG can be affected by x_l and P_{fc}. δ' and m' can be quickly adjusted by the control strategy of the SSSC, characterized by the varying x_{sc} (the equivalent series reactance of the SSSC), as well as x_l, while $\dot{\boldsymbol{V}}_{sc}$ will be dynamically modified and V'_{dc} can be stabilized simultaneously under small disturbance. Hence, the generator operating environment will be changed into a new steady operation state, characterized by the variation of generator electromechanical torque after the installation of the SSSC under small disturbance. The state matrix is also closely related to the SOFC output. Therefore, it's significant to analyze the impact of x_l and P_{fc} on the stability of the hybrid renewable energy system equipped with an SSSC.

3.2. Analysis of dynamic interactions

The parameters, x_l and P_{fc}, are closely related to the stability of the hybrid renewable energy system equipped with an SSSC, and the physical description of what affects the improvement of the stability will be presented hereafter.

Suppose that $\lambda_i = \sigma_i \pm \mathrm{j}\omega_i$ represents eigenvalues of $\boldsymbol{A}'$, $i = 1, 2, 3, \ldots, 12$. The sum of all the eigenvalues of $\boldsymbol{A}'$ is equal not only to the sum of the real parts of these eigenvalues based on the algebraic theory, but also to the sum of diagonal elements of $\boldsymbol{A}'$. Hence, the sum of all the eigenvalues, $\sum_{o\lambda}$, defined as the total damping of an open-loop system which is equal to the total damping of a closed-loop system, is written as:

$$\sum_{o\lambda} = \lambda_1 + \lambda_2 + \cdots + \lambda_{11} + \lambda_{12} = \sigma_1 + \sigma_2 + \cdots + \sigma_{11} + \sigma_{12} = a_{11} + a_{22} + \cdots + a_{11,11} + a_{12,12}, \tag{15}$$

where a_{ii} is the element of matrix $\boldsymbol{A}'$.

From the calculation, it can be seen that x_l and P_{fc} are included in a_{33} and $a_{12,12}$:

$$\begin{cases} a_{33} = -\dfrac{K_{eq}}{T'_{d0}} = -\dfrac{\left(1 + (x_d - x'_d) f_{42}\right)}{T'_{d0}} \\ a_{12,12} = \dfrac{-(a_1 + a_4 f_{53} + a_5 f_{23})}{C_{dc}} = \dfrac{-\left(\dfrac{P_{fc}}{V_{dc}^2} + km\cos\psi f_{53} + km\sin\psi f_{23}\right)}{C_{dc}} \end{cases}, \tag{16}$$

in which

$$\begin{cases} f_{42} = \dfrac{(x_s x_l + x_{tw} x_s + x_l x_{tw})}{\left((x_s x_l + x_{tw} x_s + x_l x_{tw})\left(x'_d + x_{ts}\right) + x_l x_s x_{tw}\right)} \\ f_{53} = \dfrac{km\sin\psi\left(x_l x'_d + x_l x_{ts} + x'_d x_{tw} + x_{tw} x_{ts} + x_{tw} x_l\right)}{\left((x_s x_l + x_{tw} x_s + x_l x_{tw})\left(x'_d + x_{ts}\right) + x_l x_s x_{tw}\right)} \\ f_{23} = -\dfrac{km\cos\psi\left(x_l x_q + x_l x_{ts} + x_q x_{tw} + x_{tw} x_{ts} + x_{tw} x_l\right)}{\left((x_s x_l + x_{tw} x_s + x_l x_{tw})\left(x_q + x_{ts}\right) + x_l x_s x_{tw}\right)} \end{cases}. \tag{17}$$

When x_l or P_{fc} is changed, a diagonal element of $\boldsymbol{A}'$ remains constant except for a_{33} and $a_{12,12}$. So we can analyze the trend of the total damping by analyzing a_{33} and $a_{12,12}$ when x_l or P_{fc} is changed. In addition, it should be noticed that the equivalent reactance x_l decreases as the series compensation level increases. The f_{42} increases as the x_l decreases, which means the absolute value of a_{33} increases equivalently, the same as $a_{12,12}$. Hence, the absolute value of $\sum_{o\lambda}$ will increase, which means the total damping increases as the series compensation level increases. When P_{fc} increases, the absolute value of $a_{12,12}$ increases, too. Therefore, the stability of the hybrid renewable energy system equipped with an SSSC will be improved when the series compensation level increases and the SOFC power output level increases.

4. Case studies

Test System I: SMIB. The simple but sufficient a single-machine infinite-bus (SMIB) system integrated with a DFIG-based wind farm (22 MW) and SOFC power plant (111 MW), as depicted in Fig. 1, is studied for demonstrating and evaluating the effects of an SSSC on the stability of the hybrid renewable energy system. The parameters of x_d, x_q and x'_d of the SG are 1.81 p.u., 1.76 p.u., and 0.3 p.u., and the inductance of the line which joins the SSSC is 0.5 p.u.

4.1. The impact of SSSC capability

To investigate the effects of the SSSC capability on improving the small-signal stability and transient performance of the SMIB, four various compensation levels, i.e., 0% (Case 1), 25% (Case 2), and 45% (Case 3), are examined. The partial results of eigenvalues oscillatory modes as well as eigenvalues, damping, frequency and dominant states are shown in Table 1. In order to ease the analysis, only the dominant eigenvalues (λ) related to the oscillatory modes are presented

in this paper. From the results in Table 1, it is known that δ, ω of the SG (G1) are the dominant states for mode 1 (electro-mechanical mode). E'_q, E_{qe} of the SG are dominant states for mode 2 (exciter mode). Hence, when with SSSC equipped, the change of the damping ratio (ζ) of mode 1 is not significant, attempting to lessen stability, but not exceeding its stability limit, whereas the damping ratio of mode 2 tends to increase obviously, which shows that the stability of the system increases with the increase of the series compensation level. The equivalent reactance x_l decreases as the series compensation level increases. It can also be concluded from the results that the total damping ratio, the sum of the electro-mechanical and exciter oscillatory modes, tend to increase from 18.83% to 19.88% and 21.11% in accordance with variations of series compensation levels, which means the power system stability will be improved under Case 2 and Case 3. Case 3 is the best, as shown in Fig. 5.

Table 1. Oscillatory modes under different cases in SMIB

Mode	Case	λ	ζ / %	f / Hz	Dominant states
1	Case 1	−0.1563 ± j6.5022	2.40	1.0352	δ, ω
	Case 2	−0.1569 ± j6.7154	2.34	1.0691	
	Case 3	−0.1587 ± j6.9409	2.29	1.1050	
2	Case 1	−0.5556 ± j3.3367	16.43	0.5384	E'_q, E_{qe}
	Case 2	−0.5696 ± j3.1971	17.54	0.5168	
	Case 3	−0.5852 ± j3.0544	18.82	0.4950	

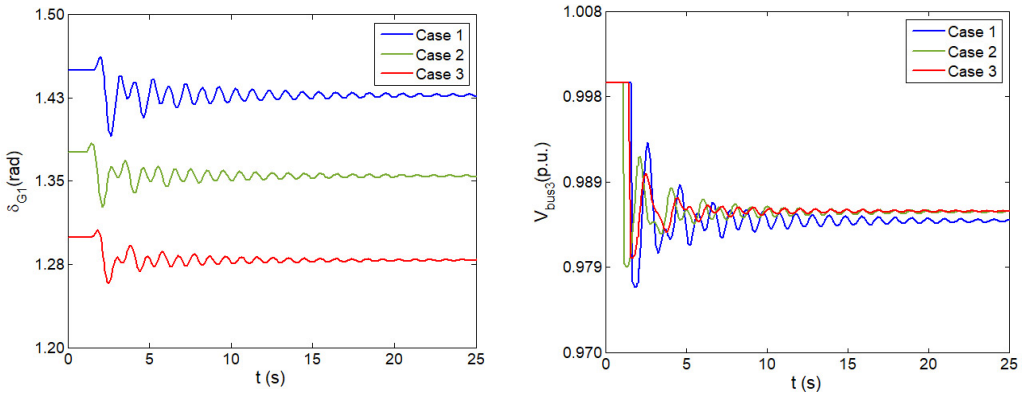

(a) (b)

Fig. 5. Transient response of the studied SMIB system subject to a three-phase short-circuit ault at the infinite bus: δ_{G1} (a); V_{bus3} (b)

Suppose that a three-phase grounding short-circuit fault occurs in the infinite bus at $t = 2$ s and the fault last for 1 s. Fig. 5 plots the comparative dynamic time-domain simulations of the

studied SMIB system without the SSSC and with the SSSC in accordance with variations of series compensation levels. It is clearly seen that the transient responses with the SSSC can get back to their original or new steady states quickly. In addition, the SSSC can offer better damping characteristic to the electro-mechanical oscillatory mode and exciter mode of the SG to damp out low-frequency oscillation, as shown in Fig. 5(a). The initial value of the rotor angles will become smaller and the oscillation amplitude of the first pendulum is reduced gradually when the series compensation level increases, characterized by the reduced x_l. The voltage responses shown in Fig. 5(b) demonstrate that the power flow is changed by the SSSC, and the magnitude of oscillations can be decreased obviously.

4.2. The impact of SOFC penetration

The performance of SOFC power output is addressed in this subsection. The examined SOFC power output level is from 111 to 444 MW and the dominant eigenvalues related to the oscillatory modes are investigated, as shown in Table 2. From the results in Table 2, it is known that with the increase of the SOFC power output, characterized by P_{fc}, ζ of mode 1 tends to increase, while ζ of mode 2 tends to increase as well. The results indicate that the incremental SOFC output can make oscillation eigenvalues fall into the region with a larger stability margin.

Table 2. Oscillatory modes under different SOFC output

Mode	SOFC output / MW	λ	ζ / %	Dominant states
1	111	−0.1563 ± 6.5022	2.40	δ, ω
	222	−0.1561 ± j6.5067	2.40	
	333	−0.1583 ± j6.5737	2.41	
	444	−0.1615 ± j6.5957	2.45	
2	111	−0.5556 ± j3.3367	16.43	E'_q, E_{qe}
	222	−0.5684 ± j3.3437	16.76	
	333	−0.5820 ± j3.2797	17.47	
	444	−0.5930 ± j3.2667	17.86	

Test System II: two-area system. The well-known two-area power system [26] is used for stability analysis to verify the effectiveness of an SSSC on improving power system small-signal stability and transient performance, as shown in Fig. 6. In this system, G1G4 present a group of synchronous generators that are strongly coupled, and both local and inter-area oscillation modes are researched. G1–G4 are equipped with an IEEE (Institute of Electrical and Electronic Engineer) type 1 regulator [26]. G1–G2 and G3–G4 are equipped with fast and slow exciters. An equivalent wind farm with a capacity of 30 MW is connected to Bus 6 together with an equivalent SOFC power plant with a capacity of 100 MW, via Bus 14. The SSSC is located between lines 8–9 in this paper. The parameters of x_d, x_q and x'_d of the SG are 1.8 p.u., 1.7 p.u., and 0.3 p.u., and the inductance of the line which joins the SSSC is 0.11 p.u.

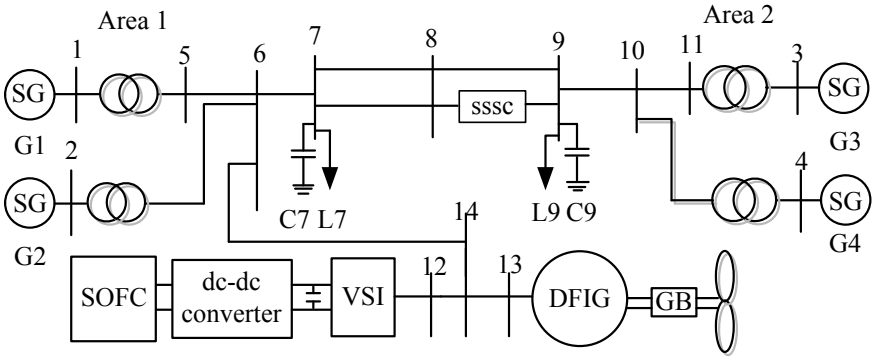

Fig. 6. Fundamental structure of a two-area

4.3. Effect of SSSC on the disturbance of tie-line power change

To investigate the effects of the SSSC capability on the disturbance of the tie-line power change of a hybrid power system connected with wind-fuel cell energy, a modified two-area power system is employed in this section, as depicted in Fig. 6. The damping oscillation modes under different degrees of the tie-line power flow are examined. For comparison purposes, the outputs of G1–G4 are adjusted under various operating conditions, and the tie-line power ranges from 303 MW to 504 MW with a series compensation level of 45%. The relevant damping characteristics of the oscillation modes are conducted in Table 3.

The relevant damping characteristics of the oscillation modes conducted in Table 3 are analyzed as follows:

1. It can be seen that there are four electro-mechanical oscillatory modes in such a two-area power system. Mode 1 is characterized by the oscillation of G1 against G2 in area 1. Mode 2 is characterized by oscillation of G3 against G4 in area 2. Mode 3 is characterized by the oscillation of G1 and G2, which are located in area 1, against G3 and G4, which are located in area 2, while mode 4 is characterized by the oscillation among G1, G2, G3, G4, and the DFIG.
2. The fifth column of Table 3 lists the difference between the damping ratio of the system with an SSSC and without an SSSC. It can be observed that when the SSSC is included in the studied system, the damping characteristics of mode 1 is slightly increased and mode 4 is considerably improved. However, the damping characteristics of mode 3 is less negative when the system is SSSC equipped, while the effect of the SSSC on mode 2 can be positive or negative in accordance with the special tie-line power.
3. Again, from the fifth column of Table 3, it is discovered that the ability of the SSSC to improve the damping characteristics of mode 1, mode 2, and mode 4 is enhanced gradually as the tie-line power increases, characterized by the increased difference, whereas the negative effect on mode 3 is strengthened. Similarly, it should be noticed that the total damping ratios of all the four electro-mechanical oscillatory modes are always incremental, as confirmed in the SMIB.

Table 3. Electro-mechanical oscillatory modes under different tie-line power

Mode	Tie-line power / MW	SSSC / %	ζ/ %	$\Delta\zeta$/ %	Dominant machines	Notes
1	393	0 45	13.7086 13.7097	0.0011	G1, G2	local mode of area 1
	480	0 45	12.6993 12.7006	0.0013		
	564	0 45	11.7677 11.7719	0.0042		
2	393	0 45	13.4520 13.4448	–0.0072	G3, G4	local model of area 2
	480	0 45	14.5744 14.5993	0.0249		
	564	0 45	15.6694 115.7533	0.0839		
3	393	0 45	8.0174 7.8612	–0.1562	G1, G3	inter area mode 1
	480	0 45	7.8697 7.6923	–0.1774		
	564	0 45	7.8678 7.6758	–0.1920		
4	393	0 45	41.0823 41.3520	0.2697	G1–G4, DFIG	inter area mode 2
	480	0 45	40.1368 40.6002	0.4634		
	564	0 45	38.8491 39.5719	0.7228		

4.4. The impact of SSSC capability on dynamic responses

In this subsection, the effectiveness of an SSSC on improving transient performance of the studied two-area power system is investigated. For comparison purpose, the tie-line power is set at 393 MW, while three various compensation levels, i.e., 0% (Case 4), 25% (Case 5), and 45% (Case 6), are examined. Suppose that a three-phase grounding short-circuit occurs in Bus 8 at t_f = 1.0 s, and is cleared at t_c = 1.1 s.

Fig. 7 plots the corresponding transient responses of the studied two-area power system under various operating conditions. It can be observed that when the supposed fault occurs, large oscillation amplitudes on all transient responses can be distinctly found. When the system is SSSC equipped, the transient responses can return to their original or new steady states more quickly, while Case 6 has the shortest recovery time. The initial value of the rotor angles shown in Fig. 7(a)

can be decreased obviously, and the magnitude of oscillations become smaller with the increase of the series compensation level. The voltage responses of the studied two-area power system shown in Fig. 7(b) illustrate that the magnitude of oscillations can also be decreased sharply when the system is SSSC equipped, especially under Case 6. Hence, the SSSC can supply more damping characteristics to damp out the inherent oscillations when the fault is suddenly applied to such a two-area power system.

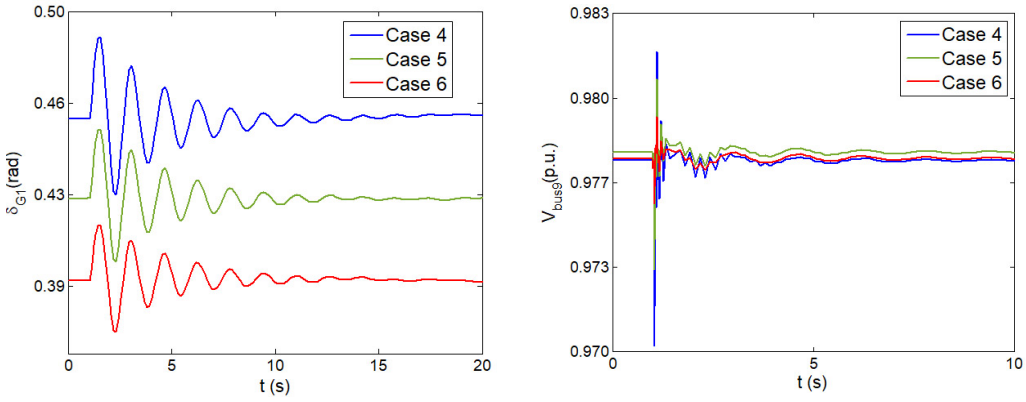

Fig. 7. Transient response of the studied two-area system subject to a three-phase short-circuit fault at Bus 8: δ_{G1} (a); V_{bus9} (b)

5. Conclusions

This paper has presented the dynamic interactions stability analysis of a hybrid renewable energy system with an SSSC. A DFIG and SOFC are considered. The linearization model of this studied hybrid single-machine infinite-bus (SMIB) power system is established. Both eigenvalue analysis and time-domain simulations with respect to a three-phase short-circuit fault, under various operating conditions, are carried out in the employed SMIB system and the two-area power system to validate the impact of dynamic interactions on suppressing inherent low-frequency oscillation and improving system stability. It can be concluded that the SOFC and SSSC are capable of enhancing the damping characteristics of the studied examples and have the ability to promote the transient performance of the studied power system. In addition, the contribution of the SSSC to supply damping characteristics is reinforced with the increase of the series compensation level set in this paper.

Acknowledgements

The authors gratefully acknowledge the research funding provided by the National Natural Science Foundation of China (NSFC) (No. 51507157), the Scientific and Technological Research Foundation of Henan Province (No. 202102210305), and the Project for University Key Teachers of Henan Province (2017GGJS093).

References

[1] Yu S.L., Fernando T., Iu H.-H.-C., *Dynamic behavior study and state estimator design for solid oxide fuel cells in hybrid power systems*, IEEE Transaction on Power Systems, vol. 31, no. 6, pp. 5190–5199 (2016).

[2] He P., Arefifar S.A., Li C.S., *Small signal stability analysis of doubly-fed induction generator-integrated power systems based on probabilistic eigenvalue sensitivity indices*, IET Generation, Transmission and Distribution, vol. 13, no. 14, pp. 3127–3137 (2019).

[3] Yang Y., Zhao J., Liu H., *A matrix-perturbation-theory-based optimal strategy for small-signal stability analysis of large-scale power grid*, Protection and Control of Modern Power Systems, vol. 3, no. 3, pp. 353–363 (2015).

[4] Liu J., Su C., Wang C., *Influence of solid oxide fuel cell on power system transient stability*, The Journal of Engineering, vol. 2019, no. 16, pp. 1081–1086 (2019).

[5] Magdy G., Shabib G., Elbaset A.A., *Optimized coordinated control of LFC and SMES to enhance frequency stability of a real multi-source power system considering high renewable energy penetration*, Protection and Control of Modern Power Systems, vol. 3, no. 3, pp. 407–421 (2018).

[6] Du W.J., Wang H.F., Cai H., *Modelling a grid-connected SOFC power plant into power systems for small-signal stability analysis and control*, International Transactions on Electrical Energy Systems, vol. 23, no. 3, pp. 330–341 (2012).

[7] He P., Wu X.X., Li C.S., *Damping characteristics improvement and index evaluation of a wind-pv-thermal-bundled power transmission system by combining PSS and SSSC*, Archives of Electrical Engineering, vol. 69, no. 3, pp. 705–721 (2020).

[8] Vikash A., Sanjeev K.M., *Power flow analysis and control of distributed FACTS devices in power system*, Archives of Electrical Engineering, vol. 67, no. 3, pp. 545–561 (2018).

[9] Bhushan R., Chatterjee K., *Effects of parameter variation in DFIG-based grid connected system with a FACTS device for small-signal stability analysis*, IET Generation, Transmission and Distribution, vol. 11, no. 11, pp. 2762–2777 (2017).

[10] Verveckken J., Silva F., Barros D., *Direct power control of series converter of unified power-flow controller with three-level neutral point clamped converter*, IEEE Transactions on Power Delivery, vol. 27, no. 4, pp. 1772–1782 (2012).

[11] Wang L., Vo Q.S., *Power Flow Control and Stability Improvement of Connecting an Offshore Wind Farm to a One-Machine In?nite-Bus System Using a Static Synchronous Series Compensator*, IEEE Transactions on Sustainable Energy, vol. 4, no. 2, pp. 358–369 (2013).

[12] Das D., Haque M.E., Gargoom A., *Operation and control of grid integrated hybrid wind-fuel cell system with STATCOM*, 22nd Australasian Universities Power Engineering Conference (AUPEC), Bali, pp. 1–6 (2012).

[13] Mahapatra S., Panda S., Swain S.C., *A hybrid firefly algorithm and pattern search technique for SSSC based power oscillation damping controller design*, Ain Shams Engineering Journal, vol. 5, no. 4, pp. 1177–1188 (2014).

[14] Al-Sarray M., McCann R.A., *Control of an SSSC for oscillation damping of power systems with wind turbine generators*, IEEE Power and Energy Society Innovation Smart Grid Technologies Conference (ISGN), Washington, USA, pp. 1–5 (2017).

[15] Darabian M., Jalilvand A., *Improving power system stability in the presence of wind farms using STATCOM and predictive control strategy*, IET Renewable Power Generation, vol. 12, no. 1, pp. 98–111 (2018).

[16] Movahedi A., Halvaei Niasar A., Gharehpetian G.B., *LVRT improvement and transient stability enhancement of power systems based on renewable energy resources using the coordination of SSSC and PSSs controllers*, IET Renewable Power Generation, vol. 13, no. 11, pp. 1849–1860 (2019).

[17] Truong D.N., Ngo V.T., *Designed damping controller for SSSC to improve stability of a hybrid offshore wind farms considering time delay*, International Journal of Electrical Power and Energy Systems, vol. 65, no. 2, pp. 425–431 (2015).

[18] Pramod Kumar, Namrata K., *Voltage control and power oscillation damping of multi-area power system using static synchronous series compensator*, Journal of Electrical and Electronics Engineering, vol. 1, no. 5, pp. 26–33 (2012).

[19] Sahu P.R., Hota P.K., Panda S., *Power system stability enhancement by fractional order multi input SSSC based controller employing whale optimization algorithm*, Journal of Electrical Systems and Information Technology, vol. 5, no. 2018, pp. 326–336 (2018).

[20] Yu Y.N., *Electric Power System Dynamics*, Academic Press Inc (1983).

[21] He P., Wen F.S., Ledwich G., *An investigation on interarea mode oscillations of interconnected power systems with integrated wind farms*, International Journal of Electrical Power and Energy Systems, vol. 78, no. 2, pp. 148–157 (2016).

[22] Wang L., Wang K.H., *Dynamic stability analysis of a DFIG-based offshore wind farm connected to a power grid through an HVDC link*, IEEE Transactions on Power Systems, vol. 26, no. 3, pp. 1501–1510 (2011).

[23] Sedghisigarchi K., Feliachi A., *Dynamic and transient analysis of power distribution systems with fuel cells-Part II: Fuel-cell dynamic model*, IEEE Transactions on Energy Conversion, vol. 19, no. 2, pp. 429–434 (2016).

[24] Benabid R., Boudour M., Abido M.A., *Development of a new power injection model with embedded multi-control functions for static synchronous series compensator*, IET Generation, Transmission and Distribution, vol. 6, no. 7, pp. 680–692 (2012).

[25] Pradhan A.C., Lehn P.W., *Frequency-domain analysis of the static synchronous series compensator*, IEEE Transactions on Power Delivery, vol. 21, no. 1, pp. 440–449 (2006).

[26] Kundur P., *Power system stability and control*, McGraw-Hill Press (1994).